

Evidence for Dyakonov-Perel spin relaxation in Gd^{3+} doped $\text{YFe}_2\text{Zn}_{20}$

M. Cabrera-Baez ^{1,2,*}, E. Padrón-Hernández ^{1,2}, M. A. Avila ³, and C. Rettori ^{3,4}

¹*Departamento de Física, Universidade Federal de Pernambuco, Recife, Pernambuco 50740-560, Brazil*

²*Pós-Graduação em Ciências de Materiais, Universidade Federal de Pernambuco, Recife, Pernambuco 50740-560, Brazil*

³*CCNH, Universidade Federal do ABC (UFABC), Santo André, São Paulo 09210-580, Brazil*

⁴*Instituto de Física “Gleb Wataghin”, UNICAMP, Campinas, São Paulo 13083-859, Brazil*



(Received 7 October 2022; revised 12 December 2022; accepted 13 December 2022; published 3 January 2023)

We report on the magnetic, thermodynamic, and electronic properties of the Gd-doped nearly ferromagnetic Fermi liquid (NFFL) system $\text{YFe}_2\text{Zn}_{20}$ by means of dc magnetic susceptibility, specific heat, and electron spin resonance (ESR) measurements. As Gd is incorporated ($\text{Y}_{1-x}\text{Gd}_x\text{Fe}_2\text{Zn}_{20}$; $x = 0.005, 0.01, \text{ and } 0.05$), the magnetization measurements present evidence of ferromagnetic correlations with unusual results in temperature-dependent ESR experiments for all samples. Strong evidence of an induced conduction ESR (CESR) is found due to the presence of Gd^{3+} ions for all of the doped samples. The usual local magnetic moment resonance associated with Gd^{3+} $4f$ localized electrons were only present for $x = 0.05$, coexisting with the CESR. Although $\text{YFe}_2\text{Zn}_{20}$ is a NFFL, no CESR was detected for the undoped sample, demonstrating the role of Gd^{3+} as a CESR activator. These results are discussed in terms of a highly polarized, enhanced Pauli paramagnetism of d -type electrons and a Dyakonov-Perel-like relaxation mechanism involving spin-flip due to magnetic impurities.

DOI: [10.1103/PhysRevB.107.014401](https://doi.org/10.1103/PhysRevB.107.014401)

I. INTRODUCTION

Relaxation time is a fundamental parameter in the understanding of magnetic systems, and together with the spin dephasing, it is a process of great importance in applied physics [1]. For example, the fact that a nonequilibrium electron spin in metals has a relatively long lifetime, allowing encoded information using the spin to travel considerable distances, is what makes spintronics an attractive source of technology [1]. Induced magnetic moments in spintronics was a central topic of various research groups exploring the spin-to-charge current conversion of metals and semimetals coupled with magnetic materials, such as the ferrimagnetic insulator yttrium iron garnet (YIG) and the ferromagnetic (FM) metal permalloy (Py) [2–5]. Noble metals such as Pd were used to study this magnetic moment induction because the large magnetic susceptibility favors the magnetic proximity effect [6] when a magnetic material such as YIG is used [7]. Those results highlight correlated systems as possible candidates to improve the spin Hall angle, which plays an important role in spintronics [7].

For mobile electrons in a metal, the spin relaxation time T_1 (often called spin-lattice or longitudinal time) and spin dephasing time T_2 (often called decoherence or transverse time) are well defined through the equations of spin precession, diffusion, and decay of the electronic magnetization under an applied magnetic field [8]. Moreover, it is well accepted that $T_2 \approx T_1 = \tau_{sf}$ (spin-flip) for metallic systems [1]. Together with τ_{sf} , another important parameter that characterizes the effectiveness of spin transport is the momentum-relaxation time τ_p (from resistivity, $\rho = m^*/ne^2\tau_p$, with m^* the effective

mass, e the charge of the conduction electrons (ce), and n the electronic density), which must be very small compared with τ_{sf} to evaluate their utility in spintronics [9].

Two distinct spin-orbit (SO) mechanisms can contribute to τ_{sf} in materials, known as Elliott-Yafet (EY) [10,11] and Dyakonov-Perel (DP) [12]. EY relaxation involves scattering on impurities and phonons producing SO band mixing, which causes a proportionality between the momentum scattering rate τ_p and the spin relaxation rate τ_{sf} [10,11]. DP relaxation involves spin precession around an effective SO field, mainly observed in noncentrosymmetric systems and leading to a motional-narrowing effect which gives τ_{sf} inversely proportional to τ_p [12]. Interfaces and bulk effects present fundamental challenges in the analysis of the SO interaction. Spin relaxation at the interfaces affects the determination of the spin diffusion length λ , the length scale related to the relaxation of spin polarization away from its source, $\lambda = \sqrt{v_F l \tau_{sf} / 3}$ (v_F is the Fermi velocity and l the mean free path) that, along with interfaces with ferromagnets, directly affects the temperature-dependent contribution of the proximity-induced magnetism [9].

Conduction electron spin resonance (CESR) experiments, together with temperature-dependent magnetoresistance, are crucial to estimate the spin-flip time τ_{sf} [9,13]. Using the CESR line width (ΔH) in the former and λ in the latter, combined with the resistivity ρ , can provide crucial interpretations of the involved mechanisms. However, the detection of CESR is sometimes not straightforward. Occasionally, an external magnetic agent may be used to polarize the ce and facilitate their resonance detection, as was the case with Au and Cu slabs (covered on each side [13] or one side [14] by a thin FM film) in transmission CESR (TCESR) setups.

$\text{YFe}_2\text{Zn}_{20}$ is a similar system to elemental Pd in terms of correlation, being characterized as a nearly FM Fermi liquid

*michael.cabrera@ufpe.br

(NFFL) [15] with $Z = 0.88$ [16], featuring enhanced magnetic susceptibility ($\chi \approx 1.8 \times 10^{-3}$ emu/mol at $T = 300$ K) [17], a Sommerfeld coefficient of $\gamma = 53$ mJ mol $^{-1}$ K $^{-2}$, and magnetic effective moment of $\mu_{\text{eff}} = 1.1 \mu_{\text{B}}/\text{Fe}$ [16]. In this case, the large e - e correlations are not sufficient to split the ce band but are large enough to make the compound exhibit strongly enhanced Pauli paramagnetism [16]. Motivated by such an enhanced magnetic susceptibility, we have detected and investigated CESR in $\text{YFe}_2\text{Zn}_{20}$. Our results suggest an alternative way for future exploration of various compounds of the $\text{RT}_2\text{Zn}_{20}$ family using ce as a local probe, providing access to the involved relaxation time. Consequently, it is possible to evaluate complex correlated materials and their applicability in spintronics.

II. EXPERIMENTAL METHODS

Batches of $\text{Y}_{1-x}\text{Gd}_x\text{Fe}_2\text{Zn}_{20}$ single crystals ($0 \lesssim x \leq 0.05$) were grown by the standard self-flux method [18,19] using an excess of Zn. The constituent elements were 99.99% Y (Ames), 99.9% Gd, 99.9% Fe, and 99.9999% Zn (Alfa-Aesar). Initial ratios of elements were 1:2:47 for the pure ternary Y : Fe : Zn, and $1 - x:x:2:47$ for the pseudoquaternaries Y : Gd : Fe : Zn. The initial reagents were sealed in an evacuated quartz ampoule and heated in a box furnace. Crystals were grown by slowly cooling the melt between 1000 and 600 °C over 100 h. At 600 °C, the ampoules were removed from the furnace, inverted, and placed in a centrifuge to spin off the excess flux, following previous reports [17]. The Gd concentration was estimated using dc magnetic susceptibility measurements assuming an effective magnetic moment of $7.94 \mu_{\text{B}}$ for Gd^{3+} . The estimated Gd concentrations were in very good agreement with the nominal ones for each sample and in agreement with previous studies [20]. X-ray powder diffraction of crushed crystals at room T was performed to determine the crystal structures, which were found consistent with previous data for the $\text{CeCr}_2\text{Al}_{20}$ -type cubic structure [20,21]. For the magnetic susceptibility ($\chi = M/H$) measurements, we used a Quantum Design Superconducting Quantum Interference Device Magnetometer (MPMS3-SQUID) at various applied magnetic fields ($H \leq 1$ T) and temperatures ($2.0 \text{ K} \leq T \leq 310 \text{ K}$). The T -dependent specific heat (C_p) was measured in a Quantum Design Physical Properties Measurement System (PPMS) using the relaxation technique at zero field. For the electron spin resonance (ESR) experiments, single crystals were crushed into fine powders of particle size $> 100 \mu\text{m}$, corresponding to an average grain size (d) larger than the skin depth (δ), $\lambda_s = d/\delta \gtrsim 10$. The X-Band ($\nu \approx 9.4$ GHz) ESR experiments were carried out in a conventional reflection CW Bruker-ELEXSYS 500 ESR spectrometer using a TE_{102} cavity. The sample temperature was changed using a helium gas-flux coupled to an Oxford T controller.

III. EXPERIMENTAL RESULTS

Figure 1 shows $C_p/T \times T^2$ for $\text{Y}_{1-x}\text{Gd}_x\text{Fe}_2\text{Zn}_{20}$ ($0 \lesssim x \leq 0.05$), where the system remains almost unaltered for $x = 0.005$ and 0.01 , but an enhancement occurs due to an additional magnetic component C_{mag} for $x = 0.05$. A fourfold

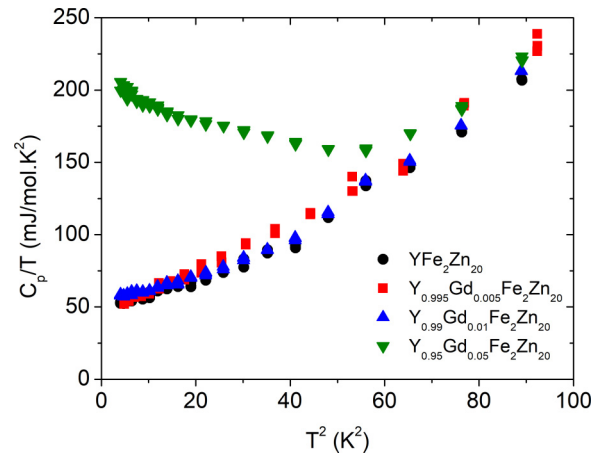


FIG. 1. C_p/T vs T^2 for $\text{Y}_{1-x}\text{Gd}_x\text{Fe}_2\text{Zn}_{20}$ ($0 \lesssim x \leq 0.05$).

increase of $C_p/T|_{T=0}$ for $T \lesssim 8$ K is clearly observed due to the interaction of localized Gd^{3+} magnetic moments in this sample.

Figure 2(a) presents dc magnetic susceptibility data. The low- T Curie-Weiss behavior indicates the presence of diluted Gd^{3+} localized magnetic moments in the $\text{YFe}_2\text{Zn}_{20}$ matrix for three concentrations ($0 \lesssim x \leq 0.05$) compatible with previous results [20]. The inset shows $\ln(\chi)$ vs $\ln(T)$ to improve the visualization of the data where strong differences were observed as Gd^{3+} enters the sample. Figure 2(b) shows the inverse of the magnetic susceptibility as a function of temperature. In the paramagnetic regime, $T \gtrsim 70$ K, a gradual decrease of the high- T slopes results from the increase in effective magnetic moment per formula unit, according to the increasing Gd^{3+} concentration (see inset). Nominal and effective concentrations were comparable with the previous study [20] of $\text{Y}_{1-x}\text{Gd}_x\text{Fe}_2\text{Zn}_{20}$ ($0 \lesssim x \leq 1$) using energy-dispersive x-ray spectroscopy, lattice constant evolution (not shown here), and CW fitted curves, which give us confidence about the effective x values of Gd. For $T \lesssim 70$ K, the system starts to show magnetic correlations, likely antiferromagnetic for $x \lesssim 0.005$ and FM for $x \gtrsim 0.01$.

Figure 3 shows the ESR at $T = 81$ K of the $\text{Y}_{0.995}\text{Gd}_{0.005}\text{Fe}_2\text{Zn}_{20}$ sample and that for its reference compound $\text{YFe}_2\text{Zn}_{20}$, both in the paramagnetic regime. A well-defined resonance with the Dysonian line shape is observed for the doped sample; however, within our ESR sensitivity, no resonance could be clearly detected for the reference compound $\text{YFe}_2\text{Zn}_{20}$, despite the enhanced Pauli-like dc magnetic susceptibility and large Stoner parameter ($Z = 0.88$, larger than Pd).

To investigate the origin of the observed resonance, we analyze the line width (ΔH), the g shift, ($\Delta g = g_{\text{exp}} - g_{\text{ins}}$), where $g_{\text{ins}} = 1.993$ is the g factor of Gd^{3+} in insulators, and the integrated intensity (Fig. 4). An increase of the linewidth at low T is revealed, contrary to the expected for a localized magnetic moment in a metallic host ($\Delta H = a + bT$) [22]. Below 20 K, the resonance suffers a strong broadening, making it difficult to perform reliable resonance analyses. The obtained Δg is positive and almost T independent [$\Delta g = 0.12(3)$] (lower inset) above $T \approx 70$ K, indicating weak FM

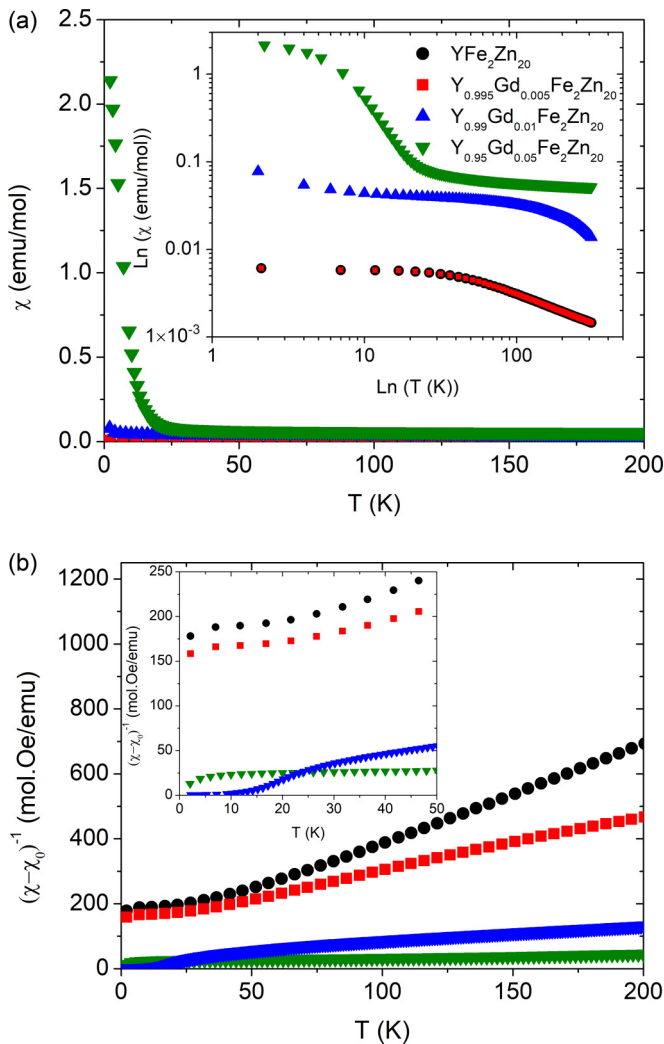


FIG. 2. Temperature dependence of the dc magnetic susceptibility and the inverse of magnetic susceptibility (inset) for $Y_{1-x}Gd_xFe_2Zn_{20}$ ($0 \lesssim x \leq 0.05$).

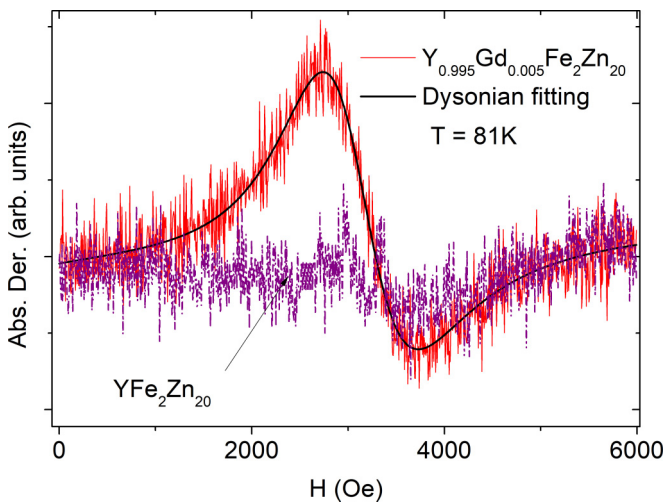


FIG. 3. Electron spin resonance (ESR) spectra of $Y_{0.995}Gd_{0.005}Fe_2Zn_{20}$ (red line) and its reference YFe_2Zn_{20} (blue line). The former shows a Dysonian conduction ESR (CESR) induced by Gd^{3+} .

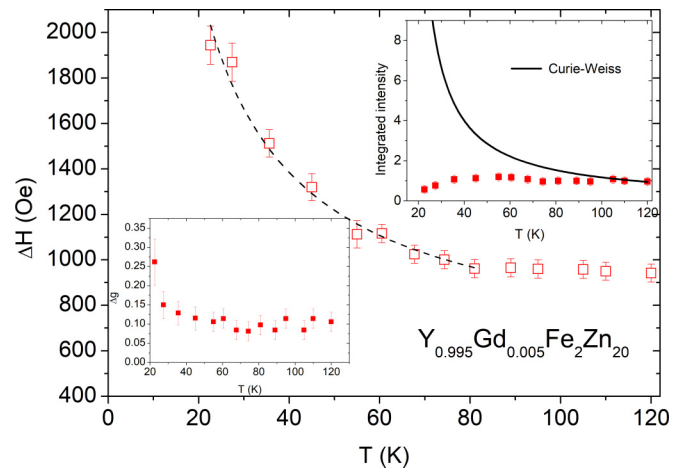


FIG. 4. Temperature dependencies of the electron spin resonance (ESR) linewidth (main graph), the integrated intensity of the ESR signal (upper inset), and the g shift (lower inset) for $Y_{0.995}Gd_{0.005}Fe_2Zn_{20}$.

local polarization caused by d -type ce . The integrated intensity of the ESR signal (top inset) is nearly T independent, characteristic of CESR, which is always proportional to the Pauli-like magnetic susceptibility of the material ($I \propto \chi_{\text{Pauli}}$) contrasting with the Curie-Weiss behavior expected for $4f$ localized magnetic moments. These results strongly suggest that the observed resonance can be safely attributed to a CESR. Hence, the magnetic doping with Gd^{3+} ions seems to activate the CESR of d -type ce without the observation of the Gd^{3+} ESR, which is unusual.

Figures 5 and 6 present the ESR spectrum and ESR parameters (ΔH , Δg , and integrated intensity) for $Y_{0.99}Gd_{0.01}Fe_2Zn_{20}$, respectively. These results show, in general, a similar trend to those found for the $x = 0.005$ sample, i.e., increase of the linewidth at low T (main graph) and a small increase of the g shift, $\Delta g = 0.15(3)$. However, there is now a slight increase of the integrated intensity toward low

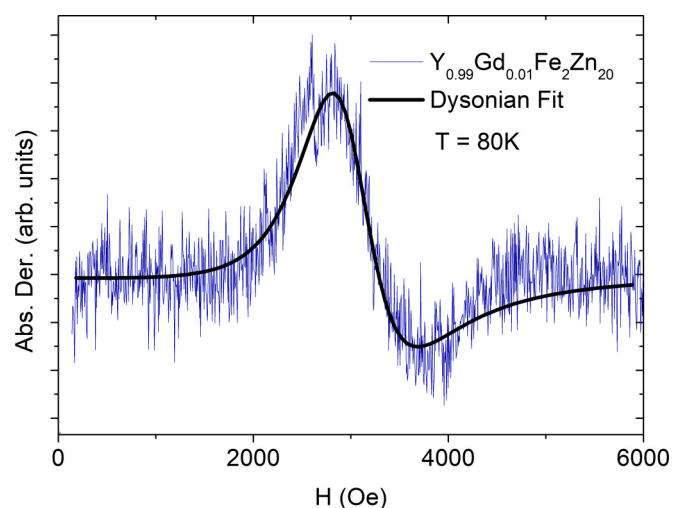


FIG. 5. Electron spin resonance (ESR) spectrum of $Y_{0.99}Gd_{0.01}Fe_2Zn_{20}$ (blue line) and respective Dysonian fitting (black line).

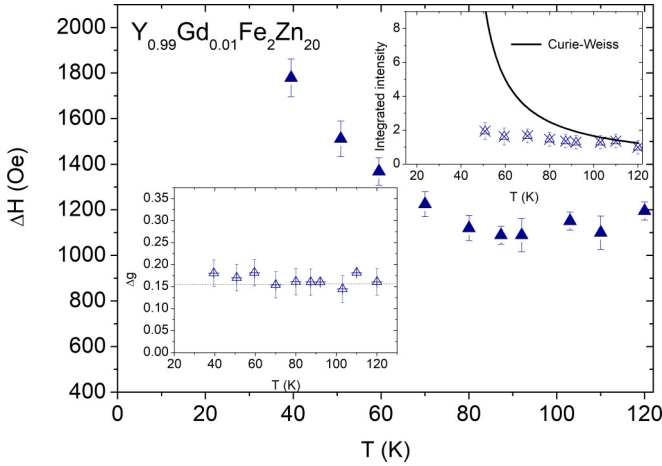


FIG. 6. Temperature dependencies of the electron spin resonance (ESR) linewidth (main graph), the integrated intensity of the ESR signal (upper inset), and the g shift (lower inset) for $Y_{0.99}Gd_{0.01}Fe_2Zn_{20}$.

T , hinting at the presence of localized magnetic moments, whereas for these first two samples, no evidence of the usual Gd^{3+} resonance was detected for $T \geq 4$ K.

Figure 7 shows the evolution of the ESR spectra for the most concentrated sample $Y_{0.95}Gd_{0.05}Fe_2Zn_{20}$ at a few representative temperatures. Above $T = 30$ K, the resonances are like those obtained for the $x = 0.005$ and 0.01 samples, i.e., a CESR (left blue dotted line). Conversely, below $T \approx 30$ K, a strong resonance coming from Gd^{3+} ions arises, with Dysonian-like line shape, as expected for Gd^{3+} ions in a metallic host and as previously reported for $GdFe_2Zn_{20}$ [23]

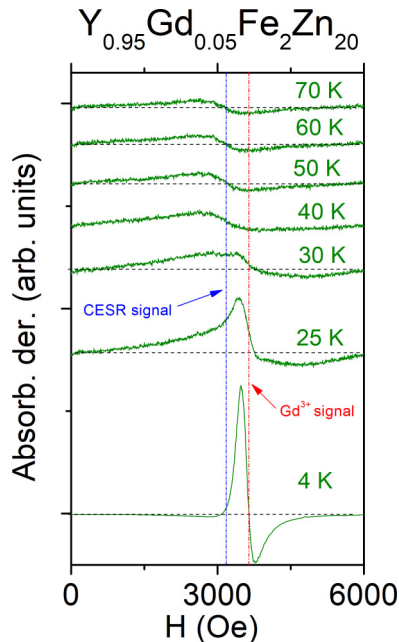


FIG. 7. Electron spin resonance (ESR) spectra at selected temperatures for $Y_{0.95}Gd_{0.05}Fe_2Zn_{20}$, showing two different resonances coming from conduction electrons and Gd^{3+} $4f$ localized electrons.

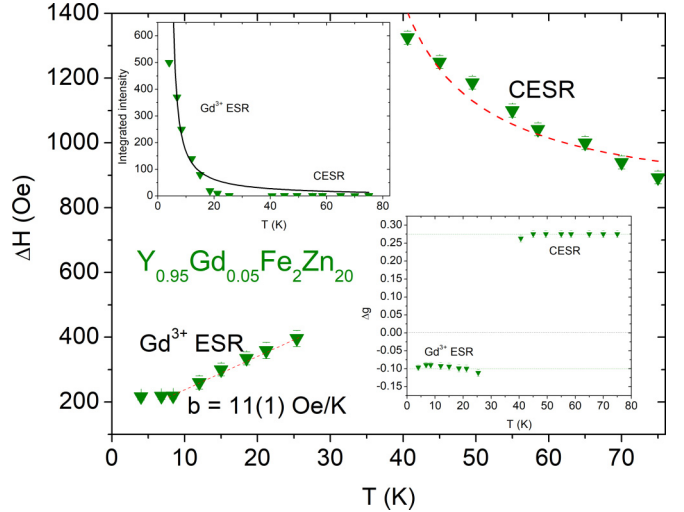


FIG. 8. Temperature dependencies of the electron spin resonance (ESR) linewidth (main graph) and the g shift (inset) for $Y_{0.95}Gd_{0.05}Fe_2Zn_{20}$.

(right red dotted line). It is noteworthy that the spectrum for $T \approx 30$ K features the coexistence of both resonances.

After extracting the ESR parameters from the full set of observed spectra, a clear distinction between a CESR and a localized ESR can be resolved. Figure 8 shows ΔH vs T (main graph), Δg vs T (lower inset) with two very well-defined regions, and the integrated intensity (upper inset) comparing CESR with Gd^{3+} ESR. Above $T \approx 30$ K, the resonance assigned to CESR presents similar features to those samples of lower Gd^{3+} concentrations. Toward low T , a broadening of the CESR and a narrowing (Korringa-like relaxation [22]) are observed for the localized magnetic moment of the Gd^{3+} ions. Moreover, the g shift of $\Delta g \sim 0.28(3)$ measured for the CESR suggests an even stronger local FM polarization caused by a mean field of d -type ce associated, again, with the presence of Gd^{3+} (see inset of Fig. 8).

In the crossover region $30 \text{ K} \lesssim T \lesssim 40 \text{ K}$, there is an overlapping of two broad resonances, making it difficult to extract the ESR parameters because both resonances coexist around $g = 2.0$. The large CESR linewidth at high T may be due to an incomplete motional narrowing [24,25] of the g -value distribution on the Fermi surface, which may also lead to some small positive g shift.

IV. ANALYSIS AND DISCUSSION

The observation and comprehension of a CESR in simple metals such as Na, Li, Ag, Cu, and Al was a subject of intense experimental and theoretical efforts in the middle of the last century [13,26–28]. Conversely, for complex metallic systems such as intermetallic compounds, it has always been a challenge to look for a CESR, which was difficult to find due to the various delicate ingredients that may contribute to its observation. Among these ingredients, we can mention (i) the intricate band structure of the material introducing a large g -value distribution [24,25], yielding an extremely broad CESR; (ii) many-body and motional narrowing effects; and (iii) small ce mean free path due to various scattering processes such as

Coulomb interaction, SO coupling (SOC), and phonons [29]. Nonetheless, it was shown that, in a simple metal such as Pd, where an electron-electron ($e-e$) exchange coupling leads to an enhanced Pauli paramagnetism (Stoner parameter $Z = 0.83$), it was possible to observe the TCESR [30]. Using the same transmission technique in FM films deposited on foils of Cu [14] and Au [13], the TCESR was observed with an enhanced resonance intensity. Based on these results and using the usual reflection technique for itinerant weak FM compounds such as ZrZn_2 , Sc_3In , and TiBe_2 , the CESR could be clearly observed [31]. However, simultaneous observation of the ESR of localized magnetic moments such as Gd^{3+} and ce in a given material was only hinted at in Ag using both techniques, transmission and reflection [32], but the presence of a bottleneck effect left an ambiguity in the identification of the observed resonances such as ce and localized magnetic moments.

Our experimental results described above assure us that a gentle increase of FM correlations of $\text{YFe}_2\text{Zn}_{20}$ allows us to observe coexistence of both resonances in $\text{Y}_{1-x}\text{Gd}_x\text{Fe}_2\text{Zn}_{20}$. Note that the T and Gd concentration dependence of both resonances are different from that of Ag : Gd [32], suggesting an unobstructed regime for this system, so we can assume that both resonances are indeed decoupled. Thus, the Gd^{3+} magnetic moments polarize the ce for all available concentrations, and the g shift increases with x , from 0.12 to 0.25 with respect to the g value of Gd^{3+} in insulators (insets in Figs. 4, 6, 8) due to their proximity. Notice that the Pd CESR g shift is $\Delta g = 0.25$ [30].

We begin with the analysis of the local moment ESR (LMESR), only present for $x = 0.05$ and below $T \approx 30$ K. The Gd^{3+} ESR linewidth broadens, following the usual linear T dependence $\Delta H = a + bT$, which leads to a Korringa-like relaxation parameter $b = 11(1)$ Oe/K. This accounts for the relaxation between the Gd^{3+} ions and ce due to exchange interaction, accompanied by a negative g shift of $\Delta g \sim -0.10(3)$, in agreement our previous work in the concentrated system $\text{GdFe}_2\text{Zn}_{20}$ [33]. This gives a ratio $b/(\Delta g)^2 \sim 1.1 \times 10^3$ Oe/K involving these two quantities, which is an order of magnitude $< 2.34 \times 10^4$ Oe/K expected for unobstructed simple metals [34]. Thus, a strong q dependence of the exchange interaction $J_{4f,ce}(q)$ may be expected for the $\text{Y}_{0.95}\text{Gd}_{0.05}\text{Fe}_2\text{Zn}_{20}$ sample, as already reported in the concentrated sample $\text{GdFe}_2\text{Zn}_{20}$ [34–36]. This is the expected behavior for a $4f$ localized magnetic moment in a complex metallic host with intricate band structure [23,33].

Let us now analyze the information coming from itinerant magnetic probes formed by the ce (CESR) present for $x = 0.005, 0.01$, and 0.05 . ESR experiments give access to important electronic properties such as τ_{sf} , from the CESR linewidth $\Delta H = \frac{2}{\gamma\tau_{sf}}$ together with the measured g shift of the ce , which is related with the spin relaxation process affected by the SO potential [10].

This particular g shift is the difference between the g value of the metal considered and the free-electron g value (2.0023) and can be taken as a rough measurement of the SO interaction if the EY relation [10,11] is fulfilled by our system.

The spin relaxation mechanism is described by the EY theory [29] as the SOC which induces spin-up and spin-down

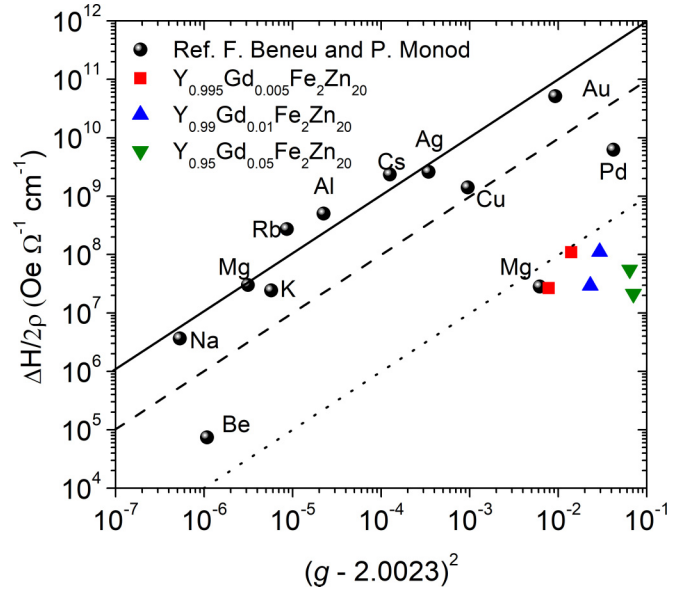


FIG. 9. Conduction electron spin resonance (CESR) linewidth divided by the resistivity for various metals (adapted from Beuneu and Monod [29]) and for $\text{Y}_{1-x}\text{Gd}_x\text{Fe}_2\text{Zn}_{20}$ vs the square of the g shift. The lines are of slope one, the dashed line corresponds to the simplest form of the Elliott relation, and the dotted line represents the line near Mg and our samples.

mixing. The admixture strength is given by the so-called SO admixture coefficient $c \propto \frac{L}{\Delta E}$, where L is the matrix element of the SOC for the conduction band and the near-lying band with an energy separation of ΔE . EY formalism establishes that momentum scattering processes induce spin transitions for the admixed states, leading to spin relaxation [Eq. (1)] and a shift in the g factor compared with the free electron [Eq. (2)] as follows [37,38]:

$$\frac{1}{\tau_{sf}} = \alpha_1 \left(\frac{L}{\Delta E} \right)^2 \frac{1}{\tau_p}, \quad (1)$$

$$\Delta g = g - g_0 = \alpha_2 \frac{L}{\Delta E}, \quad (2)$$

where α_1 and α_2 are band-structure-dependent constants. Combining both equations we obtain the so-called Elliott relation:

$$\frac{1}{\tau_{sf}} = \frac{\alpha_1}{\alpha_2^2} \frac{\Delta g^2}{\tau_p}. \quad (3)$$

The above equation correlates measurements of CESR—linewidth (related with τ_{sf}) and g shift Δg , with resistivity ρ (related with τ_p). The low-temperature dependence of $\tau_p \propto T^{-3}$, plus $\tau_{tr} \propto T^{-5}$ as the transport momentum scattering time, were included in the Elliott relation [37,38]. In such a form, the relation was explored and confirmed for Na, K, Rb, Al, Cs, Ag, Cu, and Au (solid black line of Fig. 9) but showed deviations for Be, Mg, and Pd (results digitalized from Beuneu and Monod [29]), leading to $\frac{\alpha_1}{\alpha_2^2} \approx 10$ for these metals. The dashed line represents the case of $\frac{\alpha_1}{\alpha_2^2} \approx 1$. Deviations from the Elliott relation for polyvalent metals (such as Mg and Al) were explained by enhanced SOC [39,40].

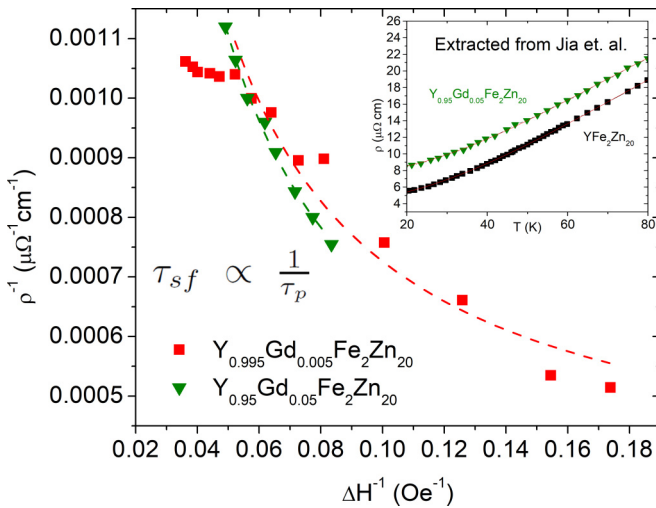


FIG. 10. $\frac{1}{\rho} (\propto \tau_p)$ vs $\frac{1}{\Delta H} (\propto \tau_{sf})$ for $Y_{1-x}Gd_xFe_2Zn_{20}$ ($x = 0.005$ and 0.05). Inset: Resistivity of $Y_{1-x}Gd_xFe_2Zn_{20}$ ($x = 0.0$ and 0.05) adapted from Jia *et al.* [20].

One way to understand the nature of the observed CESR in our system is to compare it directly with the above described CESR in those alkali metals. For this purpose, we use the measured Δg , ΔH combined with previously reported resistivity measurements [20] in the system $Y_{1-x}Gd_xFe_2Zn_{20}$ evaluated at two reference temperatures $T \approx 40$ K (upper points) and $T \approx 80$ K (lower points) and plotting $\frac{1}{2} \frac{\Delta H}{\rho} (T_{ref})$ vs $\Delta g^2 (T_{ref})$ following the Beuneu and Monod [29]. Our experimental points for the observed CESR with $x = 0.005, 0.01$, and 0.05 at these two reference temperatures were included in the comparison of alkali metals in Fig. 9 (near dotted line where $\frac{\alpha_1}{\alpha_2} \approx 0.01$), giving a clear deviation from the EY relation. This deviation was already observed in pure intermetallic systems such as MgB_2 and AlB_2 , where the linewidth does not follow the resistivity trend [41,42].

This important result raises the question about the true relaxation mechanism involved in our detected CESR. Equation (3) gives the relation $\frac{1}{\tau_{sf}} \propto \frac{1}{\tau_p}$ [37] which does not work for Gd^{3+} doped YFe_2Zn_{20} . This is expected if we consider that the system involves an internal magnetic impurity which both induces and coexists with CESR, different from the detected CESR in the explored alkali metals.

One way to evaluate the involved mechanism is to plot the dependence between τ_{sf} and τ_p . Thus, we plot $\frac{1}{\Delta H} (\propto \tau_{sf})$

and $\frac{1}{\rho} (\propto \tau_p)$ (Fig. 10), resulting in $\frac{1}{\tau_{sf}} \propto \tau_p$ like that of the DP mechanism for systems lacking inversion symmetry [12,43,44]. In the DP formalism, a momentum-dependent internal magnetic field makes the electron spin precess, with an associated frequency. The interaction between them causes flipping of the electron spins, hence spin relaxation. Although this scenario was proposed for noncentrosymmetric systems as is the case of Pt [9], in our system, the inclusion of Gd^{3+} magnetic impurities (activators of the observed CESR) may create an internal space-dependent magnetic field, causing the spin-flip. This mechanism could account for the observation of a Dysonian-like line shape with $A/B \sim 1.97$, where $\frac{T_D}{T_2} \propto \infty$. Here, T_D is the diffusion time because the *ce* remain precessing around the local magnetic field [45]. Similar behavior was observed for Pt where the EY mechanism is dominant at room temperature, but at cryogenic temperatures, the DP mechanism becomes dominant [9]. Comparing the reported values of τ_{sf} estimated for Pt at high T (13.5×10^{-15} s) and low T (16.5×10^{-15} s) with those obtained for YFe_2Zn_{20} ($\tau_{sf} \approx 1.26 \times 10^{-10}$ s for $T \geq 100$ K and $\tau_{sf} \approx 5.68 \times 10^{-11}$ s for $T \approx 20$ K), the necessity of exploring the intermetallic system YFe_2Zn_{20} for spintronic applications is clear.

V. CONCLUSIONS

In this paper, we have observed resonances with CESR features from *d*-type *ce* in YFe_2Zn_{20} induced by the addition of Gd^{3+} , allowing the characterization of local properties in this NFFL system. The local weak FM polarization of the referred electrons was monitored through the behavior of both CESR and ESR of *4f* Gd^{3+} localized electrons. This approach has allowed us to evaluate the involved relaxation mechanisms, comparing our system with the EY and DP formalisms. From our analysis, no usual EY relaxation was observed, and a DP-like relaxation is proposed as being responsible for the relaxation caused by an internal magnetic field due to the CESR activators. Our results then suggest the NFFL system YFe_2Zn_{20} as relevant to spintronics at high temperatures, based on their repercussions in the spin diffusion length λ governed by the DP mechanism.

ACKNOWLEDGMENTS

This paper was supported by Brazilian agencies FACEPE, FAPESP, CNPq, and CAPES.

- [1] I. Žutić, J. Fabian, and S. Das Sarma, *Rev. Mod. Phys.* **76**, 323 (2004).
- [2] J. B. S. Mendes, O. Alves Santos, T. Chagas, R. Magalhaes-Paniago, T. J. A. Mori, J. Holanda, L. M. Meireles, R. G. Lacerda, A. Azevedo, and S. M. Rezende, *Phys. Rev. B* **99**, 214446 (2019).
- [3] J. B. S. Mendes, A. Aparecido-Ferreira, J. Holanda, A. Azevedo, and S. M. Rezende, *Appl. Phys. Lett.* **112**, 242407 (2018).
- [4] J. B. S. Mendes, M. Gamino, R. O. Cunha, J. E. Abrão, S. M. Rezende, and A. Azevedo, *Phys. Rev. Mater.* **5**, 024206 (2021).
- [5] M. Arana, M. Gamino, E. F. Silva, V. M. T. S. Barthem, D. Givord, A. Azevedo, and S. M. Rezende, *Phys. Rev. B* **98**, 144431 (2018).
- [6] S. Y. Huang, X. Fan, D. Qu, Y. P. Chen, W. G. Wang, J. Wu, T. Y. Chen, J. Q. Xiao, and C. L. Chien, *Phys. Rev. Lett.* **109**, 107204 (2012).
- [7] T. Lin and C. Tang, and J. Shi, *Appl. Phys. Lett.* **103**, 132407 (2013).
- [8] A. Abragam and B. Bleaney, *Electron Paramagnetic Resonance of Transition Ions* (Clarendon Press, Oxford, 1970).
- [9] R. Freeman, A. Zholud, Z. Dun, H. Zhou, and S. Urazhdin, *Phys. Rev. Lett.* **120**, 067204 (2018).

- [10] R. J. Elliott, *Phys. Rev.* **96**, 266 (1954).
- [11] Y. Yafet, *Solid State Phys.* **14**, 1 (1963).
- [12] M. I. Dyakonov and V. I. Perel, *Sov. Phys. Solid State* **13**, 3023 (1972).
- [13] P. Monod and A. Janossy, *J. Low Temp. Phys.* **26**, 311 (1977).
- [14] R. H. Silsbee, A. Janossy, and P. Monod, *Phys. Rev. B* **19**, 4382 (1979).
- [15] S. Jia, S. L. Budko, G. D. Samolyuk, and P. C. Canfield, *Nat. Phys.* **3**, 334 (2007).
- [16] S. Jia, N. Ni, S. L. Bud'ko, and P. C. Canfield, *Phys. Rev. B* **80**, 104403 (2009).
- [17] S. Jia, N. Ni, G. D. Samolyuk, A. Safa-Sefat, K. Dennis, H. Ko, G. J. Miller, S. L. Bud'ko, and P. C. Canfield, *Phys. Rev. B* **77**, 104408 (2008).
- [18] P. C. Canfield and Z. Fisk, *Philos. Mag.* **B 65**, 1117 (1992).
- [19] R. A. Ribeiro and M. A. Avila, *Philos. Mag.* **92**, 2492 (2012).
- [20] S. Jia, N. Ni, S. L. Bud'ko, and P. C. Canfield, *Phys. Rev. B* **76**, 184410 (2007).
- [21] T. Nasch, W. Jeitschko, and U. C. Rodewald, *Z. Naturforsch. B* **52**, 1023 (1997).
- [22] J. Koringa, *Physica* **16**, 601 (1950).
- [23] M. Cabrera-Baez, A. Naranjo-Urbe, J. M. Osorio-Guillén, C. Rettori, and M. A. Avila, *Phys. Rev. B* **95**, 104407 (2017).
- [24] D. R. Fredkin and R. Freedman, *Phys. Rev. Lett.* **30**, 37 (1973).
- [25] R. Freedman and D. R. Fredkin, *Phys. Rev. B* **11**, 4847 (1975).
- [26] G. Feher and A. F. Kip, *Phys. Rev.* **98**, 337 (1955).
- [27] D. Lubzens and S. Schultz, *Phys. Rev. Lett.* **36**, 1104 (1976).
- [28] S. Schultz, D. R. Fredkin, B. L. Gehman, and M. R. Shanabarger, *Phys. Rev. Lett.* **31**, 1297 (1973).
- [29] F. Beuneu and P. Monod, *Phys. Rev. B* **18**, 2422 (1978).
- [30] P. Monod, *J. Phys. Colloques* **39**, C6-1472 (1978).
- [31] D. Shaltiel, *Helvetica Phys. Acta* **61**, 505 (1988).
- [32] J. M. Vargas, S. B. Oseroff, C. Rettori, *Phys. B: Condens. Matter* **404**, 2723 (2009).
- [33] M. Cabrera-Baez, M. A. Avila, and C. Rettori, *Phys. Rev. B* **98**, 165106 (2018).
- [34] D. Davidov, A. Chelkowski, C. Rettori, R. Orbach, and M. B. Maple, *Phys. Rev. B* **7**, 1029 (1973).
- [35] C. Rettori, D. Davidov, R. Orbach, E. P. Chock, and B. Ricks, *Phys. Rev. B* **7**, 1 (1973).
- [36] C. Rettori, H. M. Kim, E. P. Chock, and D. Davidov, *Phys. Rev. B* **10**, 1826 (1974).
- [37] A. Kiss, L. Szolnoki, and F. Simon, *Sci. Rep.* **6**, 22706 (2016).
- [38] L. Szolnoki, A. Kiss, L. Forro, and F. Simon, *Phys. Rev. B* **89**, 115113 (2014).
- [39] J. Fabian and S. Das Sarma, *Phys. Rev. Lett.* **81**, 5624 (1998).
- [40] J. Fabian and S. Das Sarma, *Phys. Rev. Lett.* **83**, 1211 (1999).
- [41] F. Simon, B. Dora, F. Muranyi, A. Janossy, S. Garaj, L. Forro, S. Budko, C. Petrovic, and P. C. Canfield, *Phys. Rev. Lett.* **101**, 177003 (2008).
- [42] L. M. Holanda, L. Mendonça-Ferreira, R. A. Ribeiro, J. M. Osorio-Guillén, G. M. Dalpian, K. Kuga, S. Nakatsuji, Z. Fisk, R. R. Urbano, and P. G. Pagliuso, *J. Phys.: Condens. Matter* **25**, 216001 (2013).
- [43] M. I. Dyakonov and V. Y. Kachorovskii, *Fiz. Tekh. Poluprovodn.* **20**, 178 (1986).
- [44] M. I. Dyakonov, V. A. Marushchak, and V. I. Perel, *Sov. Phys. JETP* **63**, 655 (1986).
- [45] F. J. Dyson, *Phys. Rev.* **98**, 349 (1955).